

Temperature Measurements of Laser-Cooled Ions in a Penning Trap

M. J. Jensen*, T. Hasegawa*[†] and J. J. Bollinger*

*National Institute of Standards and Technology, Boulder, CO 80305, USA

[†]Permanent address: Himeji Institute of Technology, Hyogo 678-1297, Japan

Abstract. Between 10^4 and 10^6 ${}^9\text{Be}^+$ ions are trapped in a Penning trap. The ions are laser-cooled to \sim millikelvin temperatures, where they form ion crystals. This system is an example of a strongly coupled one-component plasma. By means of Doppler laser spectroscopy we have measured the temperature and heating rate of the plasma. Initially the heating rate is low, 60 ± 40 mK/s, but after about 100 ms the plasma heats up rapidly to a few kelvin. The onset of the rapid heating coincides with the solid-liquid phase transition.

INTRODUCTION

Clouds of ions trapped in either Paul or Penning traps are routinely laser-cooled to temperatures sufficiently low for the cloud to enter the liquid or solid phases. These cold ion plasmas offer unique possibilities for studies of both atomic physics and strongly coupled plasma physics with related applications as diverse as cold antimatter, low-temperature chemistry, high-precision atomic and molecular spectroscopy, frequency standards, and quantum information processing [1]. Because the confinement in a Penning trap is provided by static electric and magnetic fields, the Penning trap is particularly well suited for trapping and cooling of large numbers of ions. We trap up to $\sim 10^6$ ${}^9\text{Be}^+$ ions in a Penning trap and laser-cool these ions to below 10 mK, where the ion cloud undergoes a phase transition to the solid phase and forms a crystal with an interparticle spacing of about $20 \mu\text{m}$ [2, 3].

A laser-cooled ion plasma in a Penning trap provides a clean, rigorous realization of a one-component plasma (OCP). An OCP is a system of a single species of classical point charges (ions) embedded in a uniform neutralizing background charge [4, 5, 6]. The thermodynamic state of an OCP is determined by the coupling parameter, Γ , which is defined as

$$\Gamma = \frac{1}{4\pi\epsilon_0} \frac{q^2}{a_{WS}k_B T}, \quad (1)$$

where ϵ_0 is the vacuum permittivity, q is the ion charge, k_B is Boltzmann's constant, T is the temperature, and a_{WS} is the Wigner-Seitz radius, given by the expression for the plasma density $n_0 = 3/(4\pi a_{WS}^3)$. Γ is a dimensionless measure of the ratio of the potential energy between nearest-neighbor ions to the ion thermal energy. Strongly

coupled OCPs are believed to exist in dense astrophysical objects such as in the crust of a neutron star, where iron nuclei are embedded in a degenerate electron gas. They can also exist in less dense objects, however only if the temperature is correspondingly low. Cold trapped ions form a convenient low-density and low-temperature strongly coupled laboratory OCP. Indeed, it has been shown that ions trapped in a Penning trap represent a rigorous realization of an OCP where the uniform neutralizing background charge is provided by the trapping potential [6, 7]. OCPs have been subject to extensive theoretical and computational studies. For instance, the coupling parameter where the plasma undergoes the liquid-solid phase transition has been determined to high accuracy. In recent years, the calculations have converged to $\Gamma \simeq 172 - 174$ [5, 8]. There is no corresponding experimental determination of this value. In fact, the actual liquid-solid phase transition has never been directly observed in an OCP.

Due to the crossed electric and magnetic fields in a Penning trap, the trapped ion plasma will undergo a rotation about the magnetic field axis. In thermal equilibrium, this rotation is rigid [6]. At the low temperatures characterizing the present work, the plasma density n_0 is constant within the plasma boundary and can be expressed as $n_0 = 2\epsilon_0 m \omega_{\text{rot}} (\Omega_c - \omega_{\text{rot}}) / q^2$, where m is the ion mass, ω_{rot} is the rotation frequency about the magnetic field axis, and Ω_c is the cyclotron frequency. Accordingly, the density is determined by the rotation frequency. At the plasma boundary, the density decreases from this constant value to zero over a distance comparable to the Debye length $\lambda_D = \sqrt{\epsilon_0 k_B T / n_0 q^2}$ which for the present system is shorter than the interparticle spacing. Due to the quadratic trapping potential, the plasma is shaped as a spheroid, the aspect ratio of which is directly related to the rotation frequency ω_{rot} . The stability region of the trap, in terms of rotation frequency, is $\omega_m < \omega_{\text{rot}} < \Omega_c - \omega_m$, where ω_m is the magnetron frequency.

Here, we present measurements of the temperature and heating rate of the trapped ions, i.e., the rate at which the temperature of the ions increases when no laser-cooling is applied. This work is motivated mainly by the prospects of creating many-particle entangled states. Entanglement can lead to improved spectroscopic precision. For an ensemble of non-entangled ions, the uncertainty on a given transition frequency scales as $1/\sqrt{N}$, where N is the number of ions; whereas for entangled ions the scaling can be as strong as $1/N$ [9, 10]. Hence, by entangling the ions the spectroscopic precision can potentially be improved by orders of magnitude. Also, entanglement is one of the key components to quantum information processing. The creation of many-particle entangled states therefore has interesting implications for experiments on quantum simulation or even quantum computation. The main technical difference between the two is that quantum computation requires that the ions can be individually addressed with a laser beam.

A necessary condition in the proposed schemes for creating entangled states is that the ions are in the Lamb-Dicke limit while their internal and motional states are being manipulated to create the entanglement [11, 12, 13]. The Lamb-Dicke limit is the limit in which the amplitude of the ion motion in the propagation direction of the state-manipulating radiation is much less than $\lambda/2\pi$, where λ is the radiation wavelength. This constraint is basically equivalent to imposing an upper limit to the ion temperature. In addition, it is not possible to carry out the desired state manipulations while directly

laser-cooling the ions. Therefore, entanglement can be obtained only if the system is cold initially and has a heating rate low enough that the ions will remain in the Lamb-Dicke limit throughout the process. Here we do not consider the option of sympathetically cooling the ions [14].

The measurements of temperature and heating rate are not only necessary to investigate the prospects of creating entangled states, but also present an opportunity to study basic properties of OCPs, in particular the solid-liquid phase transition. It will be argued that the dominant cause of heating (due to external heat sources) is collisions with the residual gas. Since the kinetic energy of the room-temperature residual gas particles by far exceeds the kinetic energy of the trapped ions, the collision energy is the same in the solid and liquid phases. Furthermore, the collisions occur on a time scale much shorter than any time scales associated with the motional modes of the ion plasma. As a result, the energy input due to the collisions is independent of whether the plasma is in the solid or liquid phase. Hence, the energy input due to residual gas collisions is constant. Accordingly, a measurement of temperature as a function of time after turning off the laser-cooling is equivalent to measuring temperature as a function of internal energy. Because the latent heat must be supplied to melt the crystal, such a measurement may show direct evidence of the solid-liquid phase transition, in the form of a short interval where the temperature remains constant despite a continuous increase in internal energy.

EXPERIMENT

A cylindrical Penning trap is used to confine between 10^4 and 10^6 ${}^9\text{Be}^+$ ions at densities on the order of 10^8 cm^{-3} [15, 16]. A schematic diagram of the setup is shown in Fig. 1. All data presented here were recorded at a pressure of $\sim 10^{-9}$ Pa. The magnetic field of 4.5 tesla is provided by a superconducting solenoid. The cyclotron frequency is $\Omega_c = 2\pi \times 7.6$ MHz, and with a typical trapping voltage $V_{\text{trap}} = 500$ V, the axial and magnetron frequencies are respectively $\omega_z = 2\pi \times 565$ kHz and $\omega_m = 2\pi \times 21$ kHz. Laser-cooling to $T < 5$ mK leads to a coupling parameter $\Gamma > 300$, and the plasma is therefore in the solid state. Cooling laser beams are sent through the center of the trap both parallel with and perpendicular to the magnetic field axis. These two cooling beams are derived from the same 313 nm beam which is produced by frequency-doubling a 626 nm beam from a dye laser. The parallel cooling beam has a wide waist of a size comparable to the diameter of the ion plasma, which is on the order of 1 mm. The waist of the perpendicular cooling beam is significantly narrower, and this beam, if offset from the center, can be used to apply a torque on the plasma and change its rotation frequency. All the diagnostics are based on fluorescence from the cooling laser beams. Real-space images of the plasma can be obtained both from the side, by use of a position-sensitive photomultiplier tube, and from the top, by use of a CCD camera equipped with an image intensifier. Phase-locked control of the rotation frequency is obtained by applying a rotating wall potential to a segmented ring electrode around the center of the trap [17]. Control of the rotation frequency implies control of the plasma density and aspect ratio.

Doppler laser-cooling was carried out on the ${}^2\text{S}_{1/2}$ ($m_1 = +\frac{3}{2}, m_J = +\frac{1}{2}$) \leftarrow ${}^2\text{P}_{3/2}$ ($m_1 = +\frac{3}{2}, m_J = +\frac{3}{2}$) transition (see Fig. 2). The parallel and perpendicular cooling beams

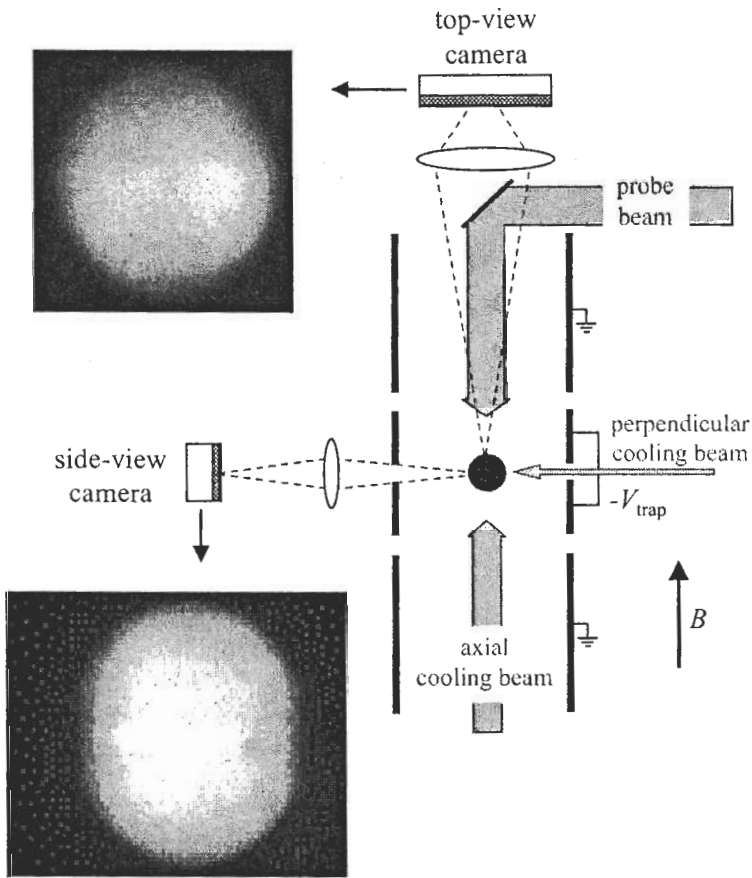


FIGURE 1. Schematic diagram of setup. Figure is not to scale. The trap diameter is 4 cm. The electrodes used to apply the rotating wall field are not shown. The vertical edges of the cloud visible in the side-view image are due to the presence of non-fluorescing impurity ions heavier than Be. The direction of the side-view light collection and the direction of the perpendicular cooling beam form a 60° angle in a plane perpendicular to the magnetic field axis.

cool the motion parallel and perpendicular, respectively, to the magnetic field axis. Due to the Coulomb interaction between the ions, there will be some coupling, and hence sympathetic cooling, between these two directions. The lowest achievable temperature using Doppler laser cooling, i.e., the Doppler cooling limit, is $T = \hbar\gamma/2k_B$, where γ is the decay rate of the upper state. For the present transition $\gamma = 2\pi \times 18$ MHz, which leads to a Doppler cooling limit of 0.43 mK. This limit is reached when the laser is detuned below the resonance by the amount $\gamma/2$. The data presented here were recorded at a larger detuning, but the dependence of the cooling limit on the detuning is relatively weak at detunings larger than $\gamma/2$, and the actual cooling limit should still be below 1 mK.

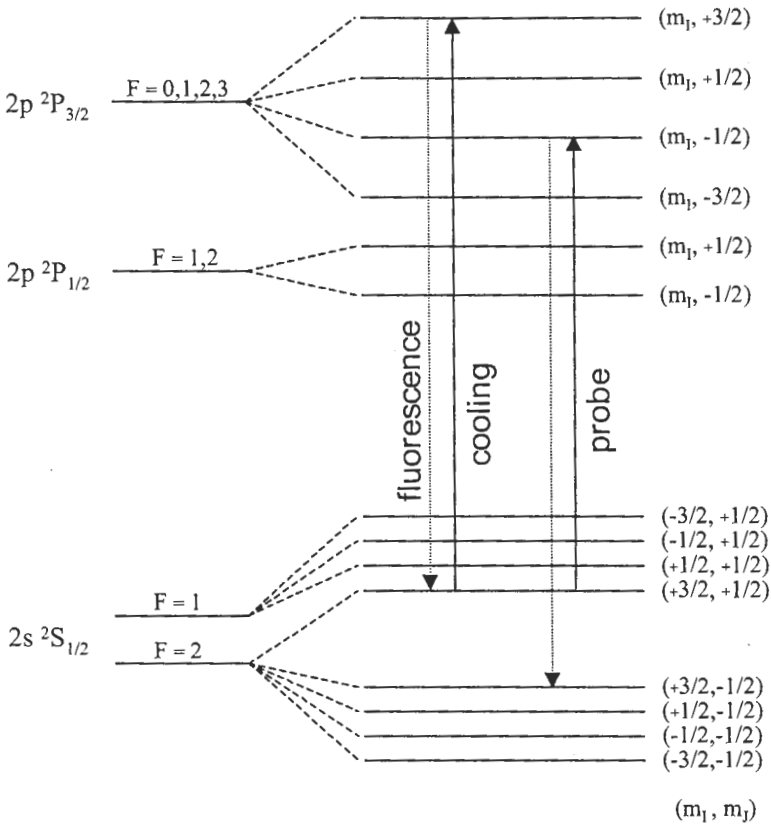


FIGURE 2. Energy-level diagram for ${}^9\text{Be}^+$ in high magnetic field (not to scale). The cooling and probe transitions are indicated. The wavelength of both laser beams is 313 nm. All diagnostics are based on the fluorescence from the cooling transition.

The temperature was probed by Doppler laser spectroscopy on the single-photon transition ${}^2\text{S}_{1/2} (m_l = +\frac{3}{2}, m_j = +\frac{1}{2}) \leftarrow {}^2\text{P}_{3/2} (m_l = +\frac{3}{2}, m_j = -\frac{1}{2})$ [18] (see Fig. 2). The probe beam was sent into the trap along the magnetic field axis, and consequently the measurement provides a determination of the axial temperature. Since the probe transition is 160 GHz below the cooling transition, a second frequency-doubled dye-laser system produces the probe beam. The upper state ${}^2\text{P}_{3/2} (m_l = +\frac{3}{2}, m_j = -\frac{1}{2})$ decays with probability $1/3$ to the ${}^2\text{S}_{1/2} (m_l = +\frac{3}{2}, m_j = +\frac{1}{2})$ state and with probability $2/3$ to the ${}^2\text{S}_{1/2} (m_l = +\frac{3}{2}, m_j = -\frac{1}{2})$ state. Hence, the resonance can be observed as a decrease in fluorescence from the cooling laser due to a depopulation of the cooling laser cycle. The data-taking procedure is as follows. At $t = 0$, the cooling laser beams are turned off. After a desired amount of time, t_{delay} , the ions are exposed to a 10 ms probe laser pulse. Immediately thereafter, the cooling laser beams are turned back on. The count rate in the side-view camera is measured before turning off (y_{before}) and after turning back on

(y_{after}) the cooling beams, and the measured signal is defined as $y_{\text{after}}/y_{\text{before}}$. After such a measurement, the ions will be exposed to the cooling beams for about 25 s in order to allow for the system to fully repump into the original state. The cooling beams will slowly move the population trapped in the $^2S_{1/2}$ ($m_I = +\frac{3}{2}, m_J = -\frac{1}{2}$) state back to the cooling transition. This cycle is repeated for different probe frequencies until the line profile has been recorded. Mechanical shutters are used for turning on and off the laser beams.

The resonance is described by a Voigt profile

$$V(\nu) \propto \int_{-\infty}^{\infty} du \frac{e^{-u^2}}{\left[\frac{\nu-\nu_0}{\Delta\nu_D} - u\right]^2 + \frac{1}{4} \left[\frac{\gamma}{2\pi\Delta\nu_D}\right]^2}, \quad (2)$$

which is a convolution between a Lorentzian and a Gaussian. ν is the laser frequency, ν_0 is the center frequency of the probe transition, and $\Delta\nu_D$ is the Gaussian width. The Lorentzian contribution, the magnitude of which is known from theory [19], is due to the natural linewidth of the transition, while the Gaussian contribution is due to Doppler broadening. A Voigt profile with a fixed Lorentzian width, $\Delta\nu_L = \gamma/2\pi = 18$ MHz, is fitted to a measured line profile and the Gaussian width $\Delta\nu_D$ is extracted from the fit. The temperature is found from the equation

$$\Delta\nu_D = \frac{\nu_0}{c} \sqrt{\frac{2k_B T}{m}}. \quad (3)$$

A correction is added to the fitting procedure to take into account saturation of the probe transition. The saturation is caused by the fact that the population in a given state is bound to be between 0 and 1. The depopulation rate of the monitored $^2S_{1/2}$ ($m_I = +\frac{3}{2}, m_J = +\frac{1}{2}$) state is proportional to the population in this state. Even at low probe laser power, we can approach the limit where almost all population is removed and the depopulation rate is significantly affected. This modifies the line profile. In the saturation correction, it is assumed that all ions are subject to the same degree of saturation. Because the waist of the probe beam is comparable to the size of the ion plasma, this assumption only holds true if the ions mix within the plasma boundary and thereby sample all possible probe laser powers. This is generally not the case, and certainly does not apply to the solid phase. However, a set of line profiles for very different probe laser powers were recorded and the Gaussian width extracted from the fits was independent of probe laser power. We therefore conclude that the error in analysis caused by the assumption of uniform saturation is negligible.

RESULTS AND DISCUSSION

Fig. 3 shows two examples of measured line profiles and corresponding Voigt profile fits. The profile recorded at $t_{\text{delay}} = 0$ is, ignoring the 10 ms duration of the probe pulse, a measure of the temperature when laser-cooling the ions. From the fit we determined a temperature of $T = 1.6 \pm 0.6$ mK which is close to the Doppler-cooling limit. The

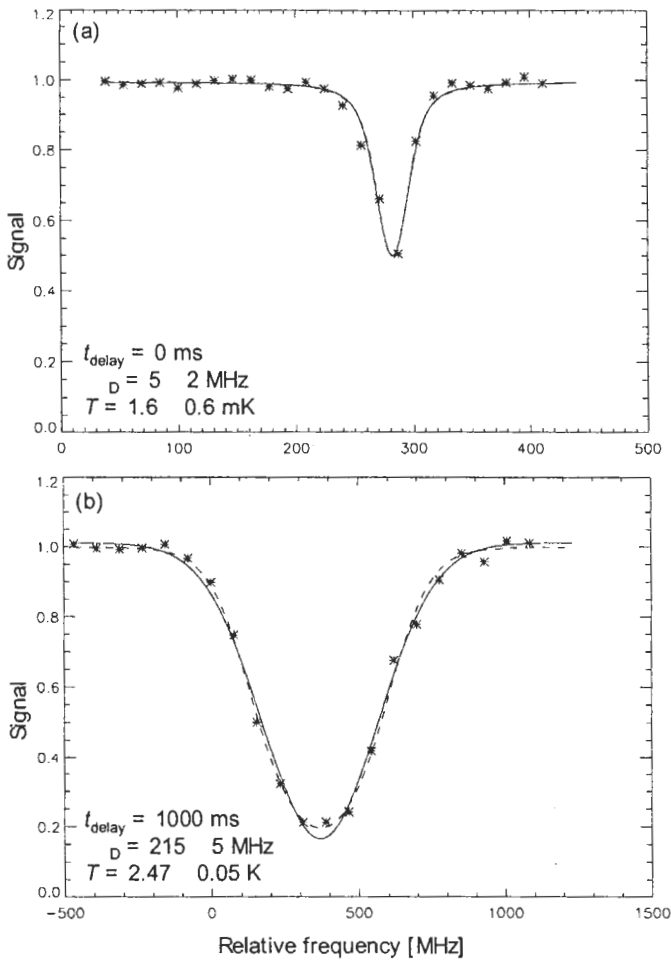


FIGURE 3. Line profiles recorded for a spherical plasma of 440,000 ions at (a) $t_{\text{delay}} = 0$ ms and (b) $t_{\text{delay}} = 1000$ ms. The dashed and solid lines are Voigt profile fits respectively with and without saturation correction. The Doppler widths and corresponding temperatures extracted from the fits with saturation correction are shown for comparison. For technical reasons, the frequency scales of figures (a) and (b) are shifted relative to each other. This shift is not due to an actual shift of the line center.

accuracy of this temperature measurement is limited by the fact that at the lowest temperatures the natural linewidth of the transition is significantly larger than Doppler width. At higher temperatures the Doppler width dominates (see Fig. 3(b)), resulting in much smaller relative uncertainties on the extracted temperatures.

Heating rate curves were obtained by measuring the temperature as a function of delay time t_{delay} after shutting the cooling laser. Fig. 4(a) shows a heating-rate curve for a plasma of 440,000 ions. Initially, the heating rate is slow. A close-up on the first 80 ms shows that the short-time heating rate is 60 ± 40 mK/s, which is consistent with

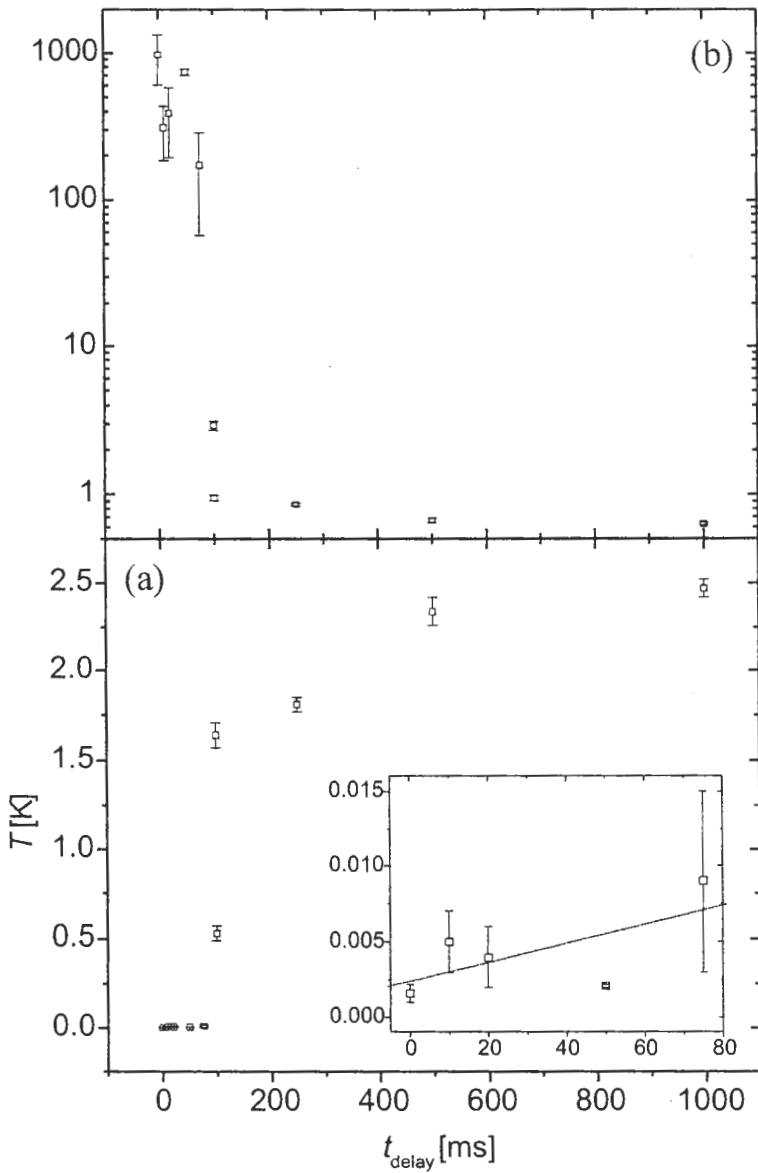


FIGURE 4. (a) Heating-rate curve (temperature as a function of t_{delay}) for a 440,000 ion cloud. A close-up of the short-time data is shown in the insert. A straight-line fit to the short-time data gives a short-time heating rate of 60 ± 40 mK/s. In the fit, we assumed equal weighting of all data points. (b) Same data set as in (a), but here plotted in terms of the coupling parameter, Γ , as a function of t_{delay} . According to theory, the solid-liquid phase transition occurs at $\Gamma \approx 170$.

the expected heating rate due to collisions with the room-temperature residual gas. This heating rate is comparable to those observed in miniature radio-frequency traps typically used for pursuing ion-entanglement experiments, although here the source of heating is different [20]. Up to four ions have been entangled in a miniature radio-frequency trap. Here, we have the possibility of entangling many more ions. Preliminary estimates indicate that it may be possible to entangle as many as 1000 ions in the present Penning trap.

At $t_{\text{delay}} \simeq 100$ ms, the temperature increases to $T \sim 2$ K within about 100 ms. The onset of this rapid heating coincides with when the coupling parameter Γ decreases to below 170 (see Fig. 4(b)), i.e., when the plasma reaches the solid-liquid phase transition. We therefore believe that the rapid heating is a signature of this transition. It is, however, not the signature expected from the latent heat. At present, we do not understand the rapid heating at the solid-liquid phase transition. We are investigating a number of ideas, with the goal of understanding the exact cause of this behavior.

ACKNOWLEDGMENTS

This research was supported by the U.S. Office of Naval Research. We gratefully acknowledge Scott Robertson and Wayne M. Itano for useful comments on this manuscript.

REFERENCES

1. Anderegg, F., Schweikhard, L., and Driscoll, C. F., editors, *Non-Neutral Plasma Physics*, AIP Conference Proceedings 606, 2002.
2. Itano, W. M., Bollinger, J. J., Tan, J. N., Jelenković, B., Huang, X.-P., and Wineland, D. J., *Science*, **279**, 686–689 (1998).
3. Mitchell, T. B., Bollinger, J. J., Dubin, D. H. E., Huang, X.-P., Itano, W. M., and Baughman, R. H., *Science*, **282**, 1290 (1998).
4. Ichimaru, S., *Rev. Mod. Phys.*, **54**, 1017 (1982).
5. Ichimaru, S., Iyetomi, H., and Tanaka, S., *Phys. Rep.*, **149**, 91–205 (1987).
6. Dubin, D. H. E., and O’Neil, T. M., *Rev. Mod. Phys.*, **71**, 87–172 (1999).
7. Malmberg, J. H., and O’Neil, T. M., *Phys. Rev. Lett.*, **39**, 1333–1336 (1977).
8. Dubin, D. H. E., *Phys. Plasmas*, **7**, 3895 (2000).
9. Wineland, D. J., Bollinger, J. J., Itano, W. M., and Heinzen, D. J., *Phys. Rev. A*, **50**, 67–88 (1994).
10. Bollinger, J. J., Itano, W. M., Wineland, D. J., and Heinzen, D. J., *Phys. Rev. A*, **54**, R4649–R4652 (1996).
11. Cirac, J. I., and Zoller, P., *Phys. Rev. Lett.*, **74**, 4091–4094 (1995).
12. Sørensen, A., and Mølmer, K., *Phys. Rev. A*, **62**, 022311 (2000).
13. Leibfried, D., DeMarco, B., Meyer, V., Lucas, D., Barrett, M., Britton, J., Itano, W. M., Jelenković, B., Langer, C., Rosenband, T., and Wineland, D. J., *Nature*, **422**, 412–415 (2003).
14. Larson, D. J., Berquist, J. C., Bollinger, J. J., Itano, W. M., and Wineland, D. J., *Phys. Rev. Lett.*, **57**, 70–73 (1986).
15. Mitchell, T. B., Bollinger, J. J., Itano, W. M., and Dubin, D. H. E., *Phys. Rev. Lett.*, **87**, 183001 (2001).
16. Kriesel, J. M., Bollinger, J. J., Mitchell, T. B., King, L. B., and Dubin, D. H. E., *Phys. Rev. Lett.*, **88**, 125003 (2002).
17. Huang, X.-P., Bollinger, J. J., Mitchell, T. B., and Itano, W. M., *Phys. Rev. Lett.*, **80**, 73–76 (1998).